Increasing of production rate of laser powder bed fusion systems

Available online at www.sciencedirect.com

ScienceDirect

Procedia CIRP 118 (2023) 699–704

www.elsevier.com/locate/procedia

16th CIRP Conference on Intelligent Computation in Manufacturing Engineering, CIRP ICME '22, Italy

Increasing of production rate of laser powder bed fusion systems

Vincenza Mercurio*, Flaviana Calignano, Marco Viccica, Luca Iuliano

Politecnico di Torino, Department of Management and Production Engineering (DIGEP) - Integrated Additive Manufacturing Center (IAM) - Corso Duca Degli Abruzzi, 24 - 10129 Torino, Italy

* Corresponding author. *E-mail address:* vincenza.mercurio@polito.it

Abstract

Laser powder bed fusion (L-PBF) is an additive manufacturing technology that allows producing complex and lightweight parts without the use of specific tooling. However, some problems limit its use in mass production. So, it is necessary to exceed the limits related to industrialization. In this study, the production rate was increased to produce AlSi10Mg alloy components and to make the process comparable to conventional casting systems. All the samples were manufactured with 90 µm layer thickness and 370 W laser power. The samples were observed to the stereomicroscope and tensile testing was carried out.

Keywords: Laser powder bed fusion; Aluminium alloy; Additive manufacturing; Process-related build-up rate

1. Introduction

Additive manufacturing (AM) refers to techniques based on adding material layer-by-layer to create the final part. Compared to conventional techniques, AM is characterized by greater freedom of design, which allows manufacturing parts with complex geometries without the use of specific tooling [1]. For this reason, additive techniques can offer both system and product benefits. As earlier AM was used just for prototyping and polymer parts, nowadays AM of metal components is used for several applications such as in automotive, electronics, aerospace and medical industries [2]. In conventional techniques, greater geometric complexity leads to an increase in production time and cost due to a greater number of process steps. The AM, on the other hand, is not subject to an increase in cost related to the complexity of the components and it could lead to a reduction in manufacturing cost and process chain [3]. Furthermore, among the advantages of AM that the industries can benefit from, there is the ability to reduce the number of parts that make up an assembled component and this implies further reducing costs [4]. In this scenario, the aerospace sector found its major applications such as manufacturing propulsion systems, structural components and fuel nozzles [2]. The automotive industry is another one of the industrial sectors interested in the applications of AM for metal parts: ever-increasing customization required from customers and reduction of vehicle weight are major objectives of the automotive sector [3,5].

The following research focuses on laser powder bed fusion (L-PBF), which is one of the AM techniques most used for manufacturing metal parts. The L-PBF is a powder bed fusion process that uses a laser beam as a heat source to selectively melt powder layer-by-layer [6]. Aluminium components made with the L-PBF technique are mostly used in the aerospace and automotive sectors. The aluminium alloys that have shown major processability are the Al–Si–Mg cast alloys, especially AlSi10Mg followed by AlSi12 [7]. Nowadays, the L-PBF process is used at the industrial production level, especially in sectors such as the dental industry or tooling manufacturing, aimed at producing small-size batches. The L-PBF systems offer high accuracy and resolution due to finer layer thickness and relatively small powder size distribution used in the process. However, these features are reflected in

10.1016/j.procir.2023.06.120

lower productivity and a slow building rate may be an obstacle to the industrialization of the process [8–10]. To raise the L-PBF technique efficiency, its build rate must be significantly increased. Among all the factors that affect the productivity and quality of L-PBF metal parts, the main process parameters that bias the process-related build-up rate $\dot{V}$ (Eq. 1) are layer thickness t [µm], scanning speed v_s [mm/s] and hatching distance h_d [mm] [10]:

$$\dot{V} = t \cdot v_s \cdot h_d \quad (1)$$

So, a trade-off between quality and productivity is necessary to reach to introduce the L-PBF systems into mass production [11]. To deal with this problem, several solutions were developed and introduced such as increasing the build volume of the machines or using multiple laser beams sources and different laser-scanning systems in one machine. All these solutions have resulted in developing and implementing more expensive L-PBF systems [8]. In literature, some studies were made on what is called High Power Selective Laser Melting (HP-SLM), whereby were used sources laser up to 1000 W and scanning speed over 2000 mm/s, using also different scanning strategies for the internal areas (with a layer thickness up to 200 µm) and the contour (with a layer thickness up to 50 µm to get better surface roughness) [9]. In another research, the hull-bulk scanning strategy was implemented to increase the L-PBF systems productivity: a 90 µm layer thickness was used for the internal areas of Ti6Al4V parts, to decrease the build time, while a 30 µm layer thickness was used for the skin to get better surface roughness and accuracy [8]. Zavala-Arredondo et al. [12] have studied the densification mechanisms of HP (1 kW) L-PBF systems of AlSi10Mg alloy changing the process parameters. Specifically, two builds were carried out with two different values of layer thickness, 50 µm and 100 µm, and a fixed value of laser power of 967 W. The L-PBF process must still overcome some challenges to meet the demands of a production reality. The novelty of this research consists in an increase of the L-PBF systems productivity keeping high the density and the mechanical properties of AlSi10Mg parts, without adapting machines with expensive solutions and using low values of laser power and high values of layer thickness. So, this study investigates the effect of the main process parameters, laser power, layer thickness, scanning speed and hatching distance, to obtain an increase in the build-up rate and to manufacture dense final parts. Furthermore, considering that the design of lightweight components often requires thin walls, two different types of tensile samples have been constructed and tested to have more information on the mechanical characteristics.

2. Material and method

2.1. Material and equipment

A gas-atomized AlSi10Mg powder, supplied by EOS GmbH German company, was used to produce the samples. The chemical composition of the powder complies with standard EN AC – 43000 [13]. Samples were produced by EOS M290 laser powder bed fusion system. The machine is equipped with a 400 W Yb fibre laser with a focus diameter of 100 µm. The processing chamber was flooded with argon to hold the oxygen content below 0.01% during the complete processing time. The scanning strategy patented by the EOS GmbH company was used in the whole study: standard stripes filled with scanning lines rotated by 67° between consecutive layers. During the work, the pre-heating temperature of the building platform was set at 200 °C.

2.2. Design of Experiments and sample processing

The design of experiments (DOE) method [14] was used to determine the effects of some parameters such as laser power, layer thickness, scanning speed and hatching distance on the density of the final parts. The laser power and layer thickness were kept fixed to 370 W and 90 µm, respectively, while the scanning speed and the hatching distance were changed (Table 1): the scanning speed ranging from 800 mm/s to 1700 mm/s, while the hatching distance ranging from 0.09 mm to 0.16 mm. A total of 32 cubic samples of 15 mm side with 32 combinations of these parameters were manufactured. After removing the building platform from the process chamber, the samples were cut from the building platform along the direction parallel to the xy-plane. Shot blasting surface treatment with glass microspheres was executed to clean the surface of samples of the unmelted powder.

Table 1. L-PBF process parameters used to manufacture the cubic samples.

Processing parameters	Value or range
Laser power [W]	370
Layer thickness [µm]	90
Scanning speed [mm/s]	800 – 1700
Hatching distance [mm]	0.09 – 0.16
Scanning strategy	Stripes rotated by 67°
Platform temperature [°C]	200

2.3. Cubic samples characterization

The relative densities of the samples were measured by Archimedes' principle with an analytical balance, KERN ABJ 320-4NM accurate to ± 0.1 mg. Each cubic sample was measured three times and then an average value of measurements was calculated. All measurements were carried out in distilled water and the influence of the temperature on fluid density was taken into account. Based on Archimedes' test results, some samples were selected to be analyzed by a stereomicroscope, LEICA S9i equipped with an integrated 10 MP camera. Therefore, a polishing operation was carried out with the MINITECH 250 SP1- PRESI manual polishing machine. After polishing treatment, the cubic samples were observed with the stereomicroscope to assess their internal porosity.

2.4. Tensile specimens characterization

The geometrical dimensions of tensile specimens and the test method were designed according to EN ISO 6892-1:2019 [15]. Therefore, uniaxial tensile tests were carried out, using an extensometer, with the universal testing machine 3MZ TENSILE model (EASYDUR) using a 10 tonnes loading cell at a strain rate of 1.5 mm/min to evaluate the mechanical properties of the material. The tensile specimens were manufactured with the combinations of scanning speed and hatching distance which have shown the best trade-off between the level of densification and the build-up rate previously determined and with both circular and rectangular sections. Specifically, the circular tensile specimens (Figure 1a) were obtained by turning cylindrical specimens constructed along the building direction (z-axis); instead, the flat test pieces were built both along the building direction (z-axis) and the direction parallel to the xy-plane and cut with wire-electrical discharge machining to the shape in Figure 1b according to the standard. It was decided to manufacture the specimens in this way to avoid the removal of support structures ruining one of the surfaces of the specimens. The mechanical properties results are the average of 5 replicas.

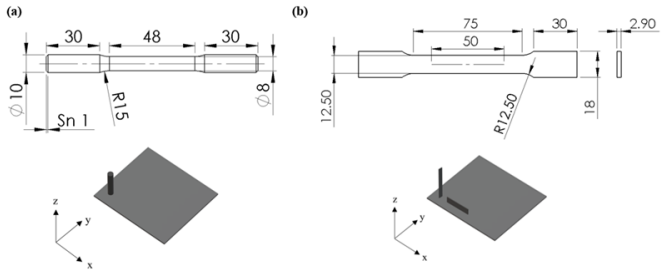

Fig. 1. (a) Circular and (b) dog-bone tensile specimens.

3. Results and discussion

3.1. Cubic samples characterization

Table 2 shows L-PBF process parameters used for manufacturing cubic samples. Values of energy density, building rate and results of density measurements are reported also. The relative density of samples was calculated using a value of theoretical density of 2.67 g/cm^3. The tested combinations of process parameters have led to values of energy density ranging from 15 J/mm^3 to 57 J/mm^3 and values of building rate ranging from 23.3 cm^3/h to 88 cm^3/h. It was already demonstrated that density is a factor influencing the mechanical properties of the L-PBF products [16]. Low values of energy density (< 21 J/mm^3) result in a low level of densification. Then, the percentage of densification increases with an increase in the values of energy density. It is probably due to the sufficient energy to melt the substrate. Further increasing the values of energy density the level of densification returns to decrease. The high energy density may cause the keyhole formation that results in the vaporization of low melting elements. Therefore, the reported data in Table 2 confirm the data found in the literature related to lower powder layers thickness [17,18].

Table 2. L-PBF process parameters and relative density measurements of all cubic samples.

Sample no.	Laser power [W]	Layer thickness [μm]	Scanning speed [mm/s]	Hatching distance [mm]	Energy density [J/mm^3]	Building rate [cm^3/h]	Relative Density [%]
1	370	90	1300	0.11	28.75	46.3	97.99
2	370	90	900	0.09	50.75	26.2	96.70
3	370	90	1400	0.09	32.63	40.8	98.09
4	370	90	800	0.09	57.10	23.3	96.18
5	370	90	1400	0.09	32.63	40.8	98.38
6	370	90	1300	0.11	28.75	46.3	98.24
7	370	90	1300	0.12	26.35	50.5	98.48
8	370	90	1400	0.12	24.47	54.4	98.50
9	370	90	900	0.13	35.14	37.9	97.13
10	370	90	1400	0.13	22.59	59.0	99.26
11	370	90	1300	0.12	26.35	50.5	98.42
12	370	90	1300	0.12	26.35	50.5	98.53
13	370	90	900	0.11	41.53	32.1	97.64
14	370	90	1400	0.12	24.47	54.4	98.56
15	370	90	1300	0.11	28.75	46.3	98.58
16	370	90	1400	0.09	32.63	40.8	98.58
17	370	90	1400	0.13	22.59	59.0	99.17
18	370	90	1400	0.13	22.59	59.0	99.13
19	370	90	1300	0.13	24.33	54.8	98.66
20	370	90	1300	0.13	24.33	54.8	98.62
21	370	90	1300	0.13	24.33	54.8	98.62
22	370	90	1700	0.16	15.11	88.1	94.74
23	370	90	1400	0.14	20.98	63.5	99.05
24	370	90	1700	0.12	20.15	66.1	98.28
25	370	90	1100	0.16	23.36	57.0	98.0
26	370	90	1700	0.12	20.15	66.1	98.14
27	370	90	1100	0.12	31.14	42.8	97.5
28	370	90	1100	0.12	31.14	42.8	98.0
29	370	90	1700	0.16	15.11	88.1	96.83
30	370	90	1400	0.14	20.98	63.5	99.15
31	370	90	1400	0.14	20.98	63.5	99.06
32	370	90	1100	0.16	23.36	57.0	98.25

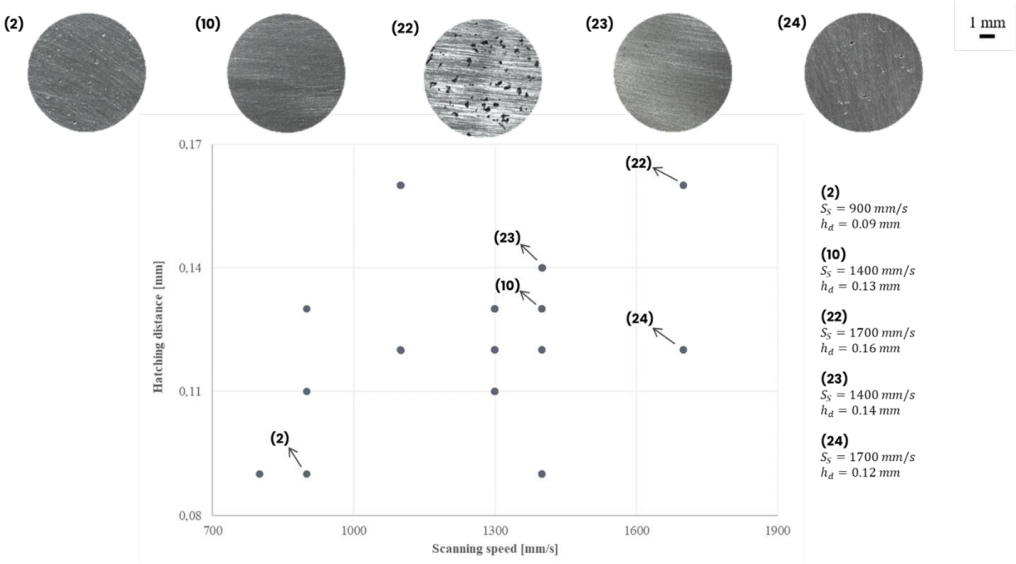

Fig. 2. Effects of changing the scanning speed and the hatching distance on the porosity. Stereomicroscopic images at 10x magnification are shown for analyzed cubic samples.

Five samples (Nos. 2, 10, 22, 23 and 24) were chosen for further analysis to better understand the correlation between process parameters and porosity. It was already demonstrated the increase in porosity by increasing the hatching distance and keeping fixed the laser power and the scanning speed [19]. Figure 2 confirms this trend: looking at couples of samples 10 – 23 and 24 – 22 with both medium and high scanning speed values it is possible to see that increasing the hatching distance increased porosity. Probably, gaps between scan tracks have formed due to the lack of sufficient overlap between intra-layer melt pools [17]. This insufficient overlap due to a determined combination of scanning speed and hatching distance values can lead not only to the presence of pores on the xy-plane but also to problems along the z-axis due to the size of the layer thickness. Furthermore, a big layer thickness may cause an incorrect fusion, as well as the porosity, which may lead to a weaker bonding between the deposited layers. It is known that the use of high values of hatching distance, scanning speed and layer thickness results in a faster production rate, but it is necessary to ensure the intra-layer and the inter-layer overlaps of the melt pools to obtain dense final components. So, a trade-off between the energy density and the manufacturing rate must be found [19]. According to the aforesaid results, the two combinations of process parameters that ensure both a good level of densification of the final parts (> 99 %) and a faster production rate are characterized by medium values of the scanning speed and the hatching distance in the investigated ranges. In particular, the parameters of sample 23, hereinafter referred to as P1, led to a build-up rate value of 63.5 cm^3/h, while the parameters of sample 10, hereinafter referred to as P2, led to a build-up rate of 59 cm^3/h. Therefore, the productivity of the process with these combinations of parameters was compared to other studies found in the literature (Table 3). It was noted that compared to studies in the literature in this work an increase in efficiency of the process up to about 64 cm^3/h was reached which is attractive to enter these technologies into mass production without reducing the relative density and mechanical characteristics of the parts. So, it is proven that the key to improving the efficiency of the process and producing large scale metal parts is increasing the layer thickness. Table 3 shows also a work in which a layer thickness of 100 µm was used to produce AlSi10Mg components, but lower values of scanning speed were needed to ensure high values of density and mechanical performances [20].

Table 3. Literature data of the productivity of L-PBF-process to manufacture AlSi10Mg parts.

Machine used	Layer thickness [µm]	Laser power [W]	Scanning speed [mm/s]	Hatching distance [mm]	Building rate [cm^3/h]	Ref.
EOS M290	30	340-390	1300	0.19-0.2	Up to 28	[25],[27]
EOS M290	40	300-370	1000-1300	0.13-0.19	Up to 35.6	[24],[26]
Other suppliers	50	350-370	930-1650	0.105-0.19	Up to 47.4	[28–34]
Other suppliers	100	350	900	0.12	38.9	[35]

3.2. Tensile specimens characterization

The mechanical properties examined were the yield strength (YS), the ultimate tensile strength (UTS) and the elongation at break. The tensile specimens were fabricated with the optimal combinations of scanning speed and hatching distance previously determined and called P1 and P2, with a bigger and a smaller value of hatching distance respectively. Table 4 shows a summary of specimens' geometry and conditions for mechanical testing.

Table 4. Geometry and conditions of the specimens investigated during the tensile test.

Parameters	Conditions of manufacturing					
	Cross-section	Production	Treatment	Building direction	No. replicas	Def.
P1	Circular	Machined	Shot blasting	z-axis	5	P1-C-Z
	Rectangular	As-built	-	z-axis	5	P1-R-Z
	Rectangular	As-built	-	xy-plane	5	P1-R-XY
P2	Circular	Machined	Shot blasting	z-axis	5	P2-C-Z
	Rectangular	As-built	-	z-axis	5	P2-R-Z
	Rectangular	As-built	-	xy-plane	5	P2-R-XY

Figure 3 shows the tensile results of all specimens investigated compared with reference values of mechanical performances of the same die-cast alloy internally collected. It is noted that all results show good reproducibility with low values of standard deviation. The mechanical properties of specimens are better or at the most comparable with specimens produced by conventional techniques, as already noted in the literature [17,32–35]. Specifically, all the specimens show very high values of YS and UTS in comparison with conventional processes. Furthermore, the standard deviation values of the machined samples are lower than in all the as-fabricated conditions. The machined conditions show values of elongation at break up to 10-12% higher than the casting conditions with lower deviations between specimens compared to as-built specimens. These lower values of standard deviation may be due to the reduction of surface defects in machined samples [34]. For the as-built conditions, the values of elongation at break increase or remain almost similar to the casting values on the xy-plane, while decrease along the z-axis, as observed in the literature [17,35]. It also analyzed the difference between the specimens manufactured in the horizontal direction (on the xy-plane) and vertical direction (along the z-axis). The main differences found in the properties are the major values of the stress and the elongation at break for all horizontal conditions. It confirms firstly the anisotropy of L-PBF-printed samples due to a directional solidification during the process [32]. In addition, it may be due to the pores in the horizontal specimens being grown in the direction of the load application, while in the vertical specimens the pores are perpendicular to the loading direction and the cross-section decreases leading to earlier collapse during the tensile test [34]. Indeed, it is noted that the horizontal direction is characterized by a better bonding between the layers and the vertical direction is weaker for L-PBF manufacturing [32,35]. One of the major advantages of additive manufacturing is to be able to produce structures porous and thin-walled parts, an example of what is called minimum feature sizes. Thin walls are most common in aerospace, automotive, aviation, electronics and railway sectors in which lightweight, corrosion resistance, high specific strength, ergonomics and high functionality are the crucial aspects [6,36,37]. Therefore, the rectangular cross-section specimens (P1-R and P2-R) were considered thin-walled parts and their mechanical behaviour was compared to other tensile specimens. Firstly, it is noted that the stress behaviour of these specimens is better than that of the parts conventionally produced (Figure 3). It was because the specimens were manufactured with the optimal process parameters that ensure a high level of densification and less internal porosity [37]. By observing the values of UTS, it can see that the values of the thin-walled samples are slightly less compared to the bulk specimens (P1-C and P2-C), with values on the xy-plane slightly greater than the values along the z-axis. Instead, the values of YS for the horizontal thin-walled specimens are also higher than the corresponding values for the bulk specimens. The trend of the values of elongation at break is almost random but their average value is closed to that of casting alloy. On balance, it can be seen that the mechanical behaviour of the thin walls is good compared to the conventionally produced parts and also to the bulk specimens.

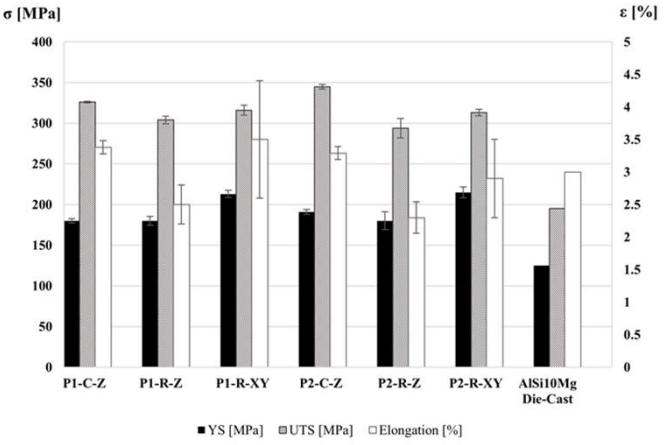

Fig. 3. Mechanical properties of L-PBF-produced AlSi10Mg tensile specimens under different conditions, compared to die-cast AlSi10Mg alloy.

4. Conclusion

This research work aimed at enhancing the efficiency of the L-PBF process without changing machines with expensive solutions or devices and decreasing densities and mechanical features of the AlSi10Mg final components. Values of relative density > 99% have been achieved with mechanical performances comparable to those of components produced with traditional casting processes. Specifically, higher values of yield strength and ultimate tensile strength were achieved. The combinations of scanning speed and hatching distance found proved to be successful in obtaining a reduction in production times without losing the quality and performance characteristics of the material.

References

[1] Tepylo N, Huang X, Patnaik PC (2019) Laser-Based Additive Manufacturing Technologies for Aerospace Applications. Adv. Eng. Mater.

[2] Singh R, Gupta A, Tripathi O, et al (2019) Powder bed fusion process in additive manufacturing: An overview. Mater Today Proc 26:3058–3070. https://doi.org/10.1016/j.matpr.2020.02.635

[3] Yi L, Gläßner C, Aurich JC (2019) How to integrate additive manufacturing technologies into manufacturing systems successfully: A perspective from the commercial vehicle industry. J Manuf Syst 53:195–211. https://doi.org/10.1016/j.jmsy.2019.09.007
[4] Fieger TV, Sattler MF, Witt G (2018) Developing laser beam welding parameters for the assembly of steel SLM parts for the automotive industry. Rapid Prototyp J. https://doi.org/10.1108/RPJ-12-2016-0204
[5] Miller WS, Zhuang L, Bottema J, et al (2000) Recent development in aluminium alloys for the automotive industry. Mater Sci Eng A 280:37–49. https://doi.org/10.1016/S0921-5093(99)00653-X
[6] Calignano F, Cattano G, Manfredi D (2018) Manufacturing of thin wall structures in AlSi10Mg alloy by laser powder bed fusion through process parameters. J Mater Process Technol 255:773–783. https://doi.org/10.1016/j.jmatprotec.2018.01.029
[7] Aboulkhair NT, Simonelli M, Parry L, et al (2019) 3D printing of Aluminium alloys: Additive Manufacturing of Aluminium alloys using selective laser melting. Prog Mater Sci 106:100578. https://doi.org/10.1016/j.pmatsci.2019.100578
[8] de Formanoir C, Paggi U, Colebrants T, et al (2020) Increasing the productivity of laser powder bed fusion: Influence of the hull-bulk strategy on part quality, microstructure and mechanical performance of Ti-6Al-4V. Addit Manuf 33:101129. https://doi.org/10.1016/j.addma.2020.101129
[9] Bremen S, Meiners W, Diatlov A (2012) Selective Laser Melting: A manufacturing technology for the future? Laser Tech J 9:33–38. https://doi.org/10.1002/latj.201290018
[10] Schleifenbaum H, Meiners W, Wissenbach K, Hinke C (2010) Individualized production by means of high power Selective Laser Melting. CIRP J Manuf Sci Technol 2:161–169. https://doi.org/10.1016/j.cirpj.2010.03.005
[11] Kose H, Jin M, Peng T (2020) Quality and productivity trade-off in powder-bed additive manufacturing. Prog Addit Manuf 5:199–210. https://doi.org/10.1007/s40964-020-00122-w
[12] Zavala-Arredondo M, London T, Allen M, et al (2019) Use of power factor and specific point energy as design parameters in laser powder-bed-fusion (L-PBF) of AlSi10Mg alloy. Mater Des 182:. https://doi.org/10.1016/j.matdes.2019.108018
[13] EOS Aluminium AlSi10Mg Material Data Sheet Metal Solutions
[14] Elsen M Van (2007) Complexity of Selective Laser Melting: a new optimisation approach
[15] ISO (2019) BSI Standards Publication Metallic materials - Tensile testing BS EN ISO 6892-1:2019
[16] Krishnan M, Atzeni E, Canali R, et al (2014) On the effect of process parameters on properties of AlSi10Mg parts produced by DMLS. Rapid Prototyp J 20:449–458. https://doi.org/10.1108/RPJ-03-2013-0028
[17] Read N, Wang W, Essa K, Attallah MM (2015) Selective laser melting of AlSi10Mg alloy: Process optimisation and mechanical properties development. Mater Des 65:417–424. https://doi.org/10.1016/j.matdes.2014.09.044
[18] Wang L zhi, Wang S, Wu J jiao (2017) Experimental investigation on densification behavior and surface roughness of AlSi10Mg powders produced by selective laser melting. Opt Laser Technol 96:88–96. https://doi.org/10.1016/j.optlastec.2017.05.006
[19] Aboulkhair NT, Everitt NM, Ashcroft I, Tuck C (2014) Reducing porosity in AlSi10Mg parts processed by selective laser melting. Addit Manuf 1:77–86. https://doi.org/10.1016/j.addma.2014.08.001
[20] Anwar A Bin, Pham QC (2017) Selective laser melting of AlSi10Mg: Effects of scan direction, part placement and inert gas flow velocity on tensile strength. J Mater Process Technol 240:388–396. https://doi.org/10.1016/j.jmatprotec.2016.10.015
[21] Nasab MH, Giussani A, Gastaldi D, et al (2019) Effect of surface and subsurface defects on fatigue behavior of AlSi10Mg alloy processed by laser powder bed fusion (L-PBF). Metals (Basel) 9:7–10. https://doi.org/10.3390/met9101063
[22] Padovano E, Badini C, Pantarelli A, et al (2020) A comparative study of the effects of thermal treatments on AlSi10Mg produced by laser powder bed fusion. J Alloys Compd 831:154822. https://doi.org/10.1016/j.jallcom.2020.154822
[23] Merino J, Ruvalcaba B, Varela J, et al (2021) Multiple, comparative heat treatment and aging schedules for controlling the microstructures and mechanical properties of laser powder bed fusion fabricated AlSi10Mg alloy. J Mater Res Technol 13:669–685. https://doi.org/10.1016/j.jmrt.2021.04.062
[24] Zhou Y, Ning F, Zhang P, Sharma A (2021) Geometrical, microstructural, and mechanical properties of curved-surface AlSi10Mg parts fabricated by powder bed fusion additive manufacturing. Mater Des 198:109360. https://doi.org/10.1016/j.matdes.2020.109360
[25] Jian ZM, Qian GA, Paolino DS, et al (2021) Crack initiation behavior and fatigue performance up to very-high-cycle regime of AlSi10Mg fabricated by selective laser melting with two powder sizes. Int J Fatigue 143:106013. https://doi.org/10.1016/j.ijfatigue.2020.106013
[26] Nadot Y, Nadot-Martin C, Kan WH, et al (2020) Predicting the fatigue life of an AlSi10Mg alloy manufactured via laser powder bed fusion by using data from computed tomography. Addit Manuf 32:100899. https://doi.org/10.1016/j.addma.2019.100899
[27] Biffi CA, Fiocchi J, Bassani P, Tuissi A (2018) Continuous wave vs pulsed wave laser emission in selective laser melting of AlSi10Mg parts with industrial optimized process parameters: Microstructure and mechanical behaviour. Addit Manuf 24:639–646. https://doi.org/10.1016/j.addma.2018.10.021
[28] Biffi CA, Fiocchi J, Tuissi A (2019) Laser Weldability of AlSi10Mg Alloy Produced by Selective Laser Melting: Microstructure and Mechanical Behavior. J Mater Eng Perform 28:6714–6719. https://doi.org/10.1007/s11665-019-04402-7
[29] du Plessis A, Beretta S (2020) Killer notches: The effect of as-built surface roughness on fatigue failure in AlSi10Mg produced by laser powder bed fusion. Addit Manuf 35:101424. https://doi.org/10.1016/j.addma.2020.101424
[30] Hofele M, Roth A, Schanz J, et al (2021) Laser Polishing of Laser Powder Bed Fusion AlSi10Mg Parts—Influence of Initial Surface Roughness on Achievable Surface Quality. Mater Sci Appl 12:15–41. https://doi.org/10.4236/msa.2021.121002
[31] Cerri E, Ghio E (2020) AlSi10Mg alloy produced by Selective Laser Melting: Relationships between Vickers microhardness, Rockwell hardness and mechanical properties. Metall Ital 112:5–17
[32] Jawade SA, Joshi RS, Desai SB (2020) Comparative study of mechanical properties of additively manufactured aluminum alloy. Mater Today Proc. https://doi.org/10.1016/j.matpr.2020.02.096
[33] Silvestri AT, Astarita A, Hassanin A El, et al (2020) Assessment of the mechanical properties of AlSi10Mg parts produced through selective laser melting under different conditions. Procedia Manuf 47:1058–1064. https://doi.org/10.1016/j.promfg.2020.04.115
[34] Tradowsky U, White J, Ward RM, et al (2016) Selective laser melting of AlSi10Mg: Influence of post-processing on the microstructural and tensile properties development. Mater Des 105:212–222. https://doi.org/10.1016/j.matdes.2016.05.066
[35] Ponnusamy P, Rashid RAR, Masood SH, et al (2020) Mechanical properties of slm-printed aluminium alloys: A review. Materials (Basel).
[36] Ahmed A, Majeed A, Atta Z, Jia G (2019) Dimensional quality and distortion analysis of thin-walled alloy parts of AlSi10Mg manufactured by selective laser melting. J Manuf Mater Process 3:. https://doi.org/10.3390/jmmp3020051
[37] Zhang Y, Majeed A, Muzamil M, et al (2021) Investigation for macro mechanical behavior explicitly for thin-walled parts of AlSi10Mg alloy using selective laser melting technique. J Manuf Process 66:269–280. https://doi.org/10.1016/j.jmapro.2021.04.022